Draft version November 2, 2012
Preprint typeset using LaTeX style emulateapj v. 5/2/11

arXiv:1208.5279v2 [astro-ph.HE] 31 Oct 2012

DYNAMICAL CAPTURE BINARY NEUTRON STAR MERGERS

William E. East and Frans Pretorius
Department of Physics, Princeton University, Princeton, NJ 08544, USA.
Draft version November 2, 2012

ABSTRACT

We study dynamical capture binary neutron star mergers as may arise in dense stellar regions such as globular clusters. Using general-relativistic hydrodynamics, we find that these mergers can result in the prompt collapse to a black hole or in the formation of a hypermassive neutron star, depending not only on the neutron star equation of state but also on impact parameter. We also find that these mergers can produce accretion disks of up to a tenth of a solar mass and unbound ejected material of up to a few percent of a solar mass. We comment on the gravitational radiation and electromagnetic transients that these sources may produce.

Subject headings: black hole physics—gamma-ray burst: general—gravitation—gravitational waves—stars: neutron

1. INTRODUCTION

Merging binary neutron stars (NSs) warrant detailed study because these systems promise to be rich sources of both gravitational and electromagnetic (EM) radiation, probing strong-field gravity and nuclear density physics. NS–NS mergers are a primary source targeted by gravitational wave (GW) detectors (such as LIGO; Abramovici et al. 1992). They are also candidates for short gamma-ray burst (SGRB) progenitors and several other EM counterparts (Metzger & Berger 2012; Roberts et al. 2011; Piran et al. 2012) which could potentially be observed by current and upcoming wide-field survey telescopes like PTF (Rau 2009), Pan-STARRS (Kaiser 2004), and LSST (LSST Science Collaborations et al. 2009).

There have been numerous studies of primordial binary NS mergers (see e.g. Faber & Rasio (2012)), which will have essentially zero orbital eccentricity when they enter the frequency band of ground-based GW detectors. However, binaries may also form via n-body interactions in dense stellar regions and some fraction of them will have sizable eccentricity at merger. A likely environment to find such binaries is globular clusters (GCs) that have undergone core collapse (Fabian et al. 1975; Grindlay et al. 2006). In Lee et al. (2010), it was argued that the rate of tidal capture and collision of two NSs in GCs (using M15 as a prototype) peaked around $z \simeq 0.7$ at values of ~ 50 yr^{-1} Gpc^{-3} (falling to ~ 30 yr^{-1} Gpc^{-3} by $z = 0$) and was consistent with the observed SGRB rate. However, this does not take into account natal kicks. A recent simulation of M15 that assumed a modest NS retention fraction of 5% found $\sim 1/4$ fewer NSs in the central 0.2 pc (Murphy et al. 2011) compared to an earlier study that ignored kicks (Dull et al. 1997, 2003), implying the above rate (scaling as the number density squared) could be overestimated by an order of magnitude. On the other hand, observations suggest that the NS retention fraction in some GCs can be as large as 20% (Pfahl et al. 2002), and the model of Lee et al. (2010) did not take into account other channels that could lead to binary merger within a Hubble time, such as Kozai resonance in a triple system (Thompson 2011).

The above discussion focused on GC environments, and similar interactions in galactic nuclei would also add to the rates (O'Leary et al. 2009; Kocsis & Levin 2012; Antonini & Perets 2012). Still, it is far from certain that high eccentricity mergers occur frequently enough to expect observation with the upcoming generation of GW detectors. However, it is also not implausible that they do, and as eccentric NS mergers may also produce distinguishable EM emission compared to quasi-circular mergers, it behooves us to understand both systems from a multi-messenger perspective.

In Stephens et al. (2011) and East et al. (2012b), black-hole–neutron-star (BH–NS) mergers formed through dynamical capture were found to exhibit a rich variation with impact parameter, in some cases producing sizable disks and amounts of unbound material. In Gold et al. (2011), several eccentric NS–NS mergers were studied using a $\Gamma = 2$ equation of state (EOS) and shown to exhibit f-mode excitation during close encounters. There have also been studies of BH–NS and NS–NS collisions with Newtonian gravity (Lee et al. 2010; Rosswog et al. 2012) showing similar variation in the outcomes.

In this Letter, we study dynamical capture NS–NS mergers for a range of impact parameters using general-relativistic hydrodynamics (GRHD). We also consider several different NS EOSs because of the uncertainty regarding the correct description of matter above nuclear densities. One of the important issues we address for the first time is if these mergers can produce hypermassive neutron stars (HMNSs). In studies of quasi-circular systems it was found that thermal energy from the merger, as well as differential rotation, could support long-lived HMNSs for some EOSs (e.g., Sekiguchi et al. 2011) and that this would be imprinted in the GW signal and resulting disk properties. HMNSs with longer lifetimes can also build up significant magnetic fields which can power strong EM transients during the collapse to a BH (Lehner et al. 2011). For dynamical capture binaries, the amount of angular momentum, and likely the amount of shock heating, will be strong functions of impact parameter, suggesting HMNS formation will be as well.

Another notable feature of dynamical capture NS–NS mergers is their potential to produce unbound nuclear material which will decompress and form heavy nuclei via the r-process (Lattimer & Schramm 1974; Rosswog et al. 1998; Li & Paczynski 1998); subsequent radioactive decay could produce observable emission. Recent work (Fischer et al. 2010; Arcones & Janka 2011) suggests processes like NS–NS mergers may be needed to supplement the supernovae r-process yield in accounting for the observed abundances. Though simulations of quasi-circular NS–NS mergers using Newtonian or conformally flat gravity have found suitable ejecta, they seem to be in tension with fully general-relativistic results which find negligible amounts of ejecta (Faber & Rasio 2012). This is *arguably* because of strong-field GR effects, such as BH formation and the existence of innermost stable orbits. As we show, dynamical capture mergers are more promising sources of ejecta, presumably as the stars are less bound when disruption occurs.

In the remainder of this Letter, we outline our methods for simulating NS–NS mergers with GRHD, discuss the merger dynamics for a range of impact parameters and three different EOSs, and comment on potential GW and EM counterparts. We find that, while the GW signals from these mergers may be challenging to detect with upcoming ground-based detectors, they have the potential to source numerous EM transients. Non-merging close encounters can induce tidal deformations strong enough to crack the NSs' crusts; a merger where the total mass is above the maximum mass of a single NS can either promptly collapse to a BH or produce a hot, rapidly rotating HMNS, where the latter outcome tends to have more massive disks and ejected material.

2. NUMERICAL APPROACH

We numerically solve the Einstein equations, discretized with finite differences, in the generalized harmonic formulation. The hydrodynamics are evolved in a conservative formulation using high-resolution shock-capturing techniques. Details are given in East et al. (2012c).

We use adaptive mesh refinement with up to seven levels that are dynamically adjusted according to truncation error (TE) estimates. To measure convergence and TE, we perform a select number of simulations at three different resolutions. The low, medium, and high resolutions, respectively, have base levels covered by 129^3, 201^3, and 257^3 points (with the maximum TE threshold adjusted accordingly), and approximately 64, 100, and 128 points across the diameter of the NSs on the finest level at the initial time (for the HB EOS). In Figure 1, we show an example of convergence of NS trajectories as well as the constraints of the field equations. All simulations are performed at medium resolution and results quoted below are from this resolution, with Richardson extrapolated values given in parenthesis (indicating the quantity's TE) where multiple resolution data are available.

We use the same gauge, slope limiters, and flux methods as in East et al. (2012b). We use the piecewise polytropic EOS models labeled 2H, HB, and B from Read et al. (2009) and include a thermal component $P_{\rm th} = (\Gamma_{\rm th} - 1)\epsilon_{\rm th}\rho$ with $\Gamma_{\rm th} = 1.5$. These EOSs

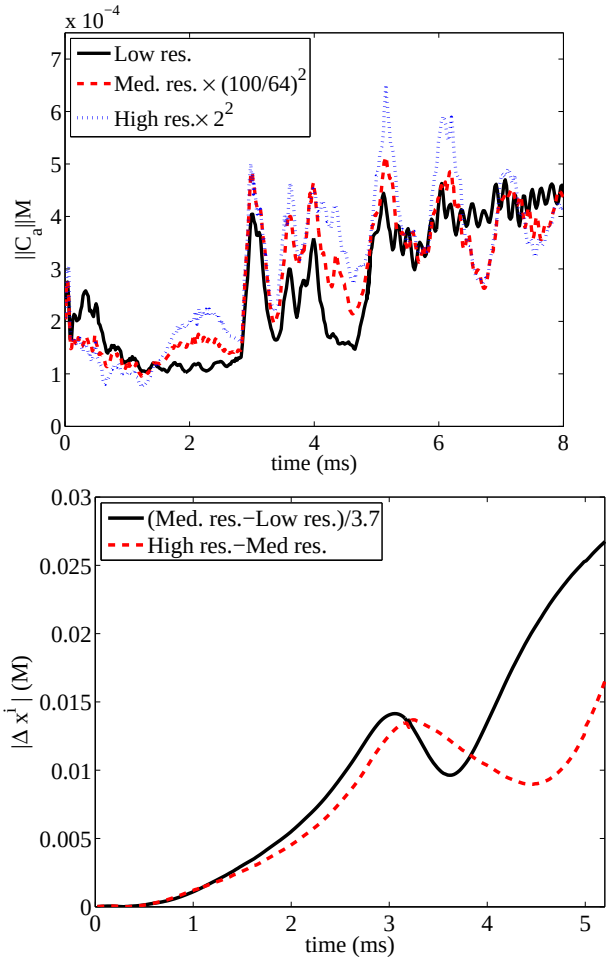

FIG. 1.— Top: L^2-norm of the constraints ($C_a \equiv H_a - \Box x_a$) in the $100M \times 100M$ region around the center of mass in the equatorial plane for the $r_p = 7.5$, HB case, with the three resolutions scaled assuming second-order convergence. Bottom: the difference in the NS center of mass as a function of time from the different resolution runs for the $r_p = 10$, HB case, scaled assuming second-order convergence.

were designed to span the range of possible EOSs. The 2H, HB, and B EOSs, respectively, give NSs with compactions $M_{\rm NS}/R_{\rm NS}$ of 0.13, 0.17, and 0.18 for $M_{\rm NS} = 1.35$ $M_\odot$ and maximum masses of 2.83, 2.12, and 2.0 $M_\odot$ (unless otherwise stated we use geometric units with $G = c = 1$).

We construct initial data by solving the constraint equations in the conformal thin-sandwich formulation as described in East et al. (2012). We begin the two NSs at a separation of $d = 50M$, where $M = 2.7$ $M_\odot$ is the total mass of the system (hence $d = 200$ km), and consider various initial velocities which we label by r_p, the periastron distances of parabolic Newtonian orbits with the same velocities (which will be different from the actual periastron distance of the simulated binaries). We performed the majority of the simulations using the middle compaction HB EOS but ran select impact parameters using all three EOSs. For all simulations except one we used NSs that both have a mass of 1.35 $M_\odot$; the other case has a mass ratio of $q = 0.8$ and a total mass of 2.88 $M_\odot$. We leave a more detailed study of mass-ratio dependence to future work.

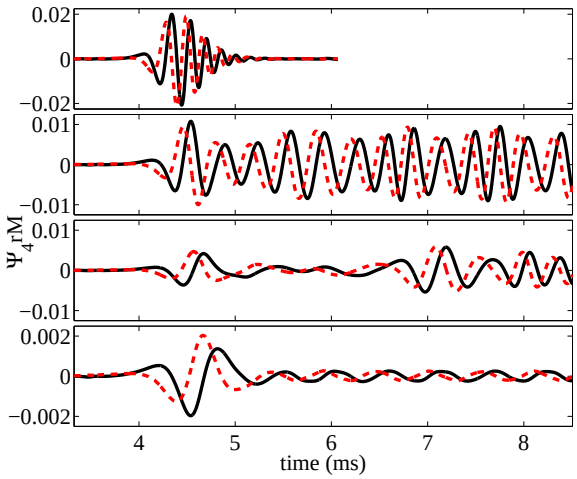

FIG. 2.— Real (solid black) and imaginary (dotted red) components of the Newman–Penrose scalar Ψ_4 on the axis orthogonal to the orbit measured at $r = 100M$ for the $r_p = 5$, 7.5, 8.75, and 10 cases with HB EOS.

3. RESULTS AND DISCUSSION

3.1. *Effect of Impact Parameter*

Using the HB EOS, we consider a range of impact parameters from $r_p/M = 2.5$ (we henceforth quote r_p in units of M) to $r_p = 20$ (i.e., 10 to 80 km). This is well within the range to form a bound system as Peters & Mathews (1963) indicate that for equal masses, GW capture occurs for $r_p \lesssim 1.8/w^{4/7}$ where w is the velocity at infinity. (Tidal energy loss (Press & Teukolsky 1977), because of the relative scalings with distance, is subdominant in determining *capture*.) Binaries that approach with small impact parameters ($r_p = 2.5$ and 5) promptly merge and collapse to a BH. For $r_p = 2.5$ the mass and dimensionless spin of the final BH is $M_{\rm BH}/M = 0.998(0.995)$ and $a = 0.537(0.538)$ while the energy and angular momentum in GWs is $E_{\rm GW}/M = 3.7(4.0)\times10^{-3}$ and $J_{\rm GW}/M^2 = 2.60(2.75) \times 10^{-2}$. For $r_p = 5$, $M_{\rm BH}/M = 0.985$, $a = 0.719$, $E_{\rm GW}/M = 1.06 \times 10^{-2}$, and $J_{\rm GW}/M^2 = 6.74 \times 10^{-2}$; Figure 2 shows the corresponding GW signals. For both these cases, the amount of material leftover after merger is $\lesssim 10^{-6}$ the original rest mass of the NSs. The dearth of matter post-merger, and the fact that most of the power of the GW signal is at a relatively high frequency (~ 5 kHz), makes these scenarios less promising sources of observable EM or gravitational radiation.

Binaries with larger impact parameters ($r_p = 10$, 15, and 20) result in non-merging close encounters followed by long elliptic orbits which we did not follow in their entirety due to limited computational resources. The close encounters result in pulses of GW radiation and excite f-mode oscillations in the stars, which are also evident in the GW signal (see Figures 2 and 3). This f-mode excitation was studied in detail in Gold et al. (2011) and also found in similar BH–NS encounters (Stephens et al. 2011; East et al. 2012b). The induced tidal ellipticity in the $r_p = 10$ case is greater than the $\delta R/R \approx 0.1$ value required to induce a strain of $u_{\rm strain} \simeq 0.1$ and shatter the NS crust (Horowitz & Kadau (2009); though we are not modeling the crust here). The energy and angular momentum radiated in the $r_p = 10$ close encounter is $E_{\rm GW}/M = 1.472(1.474) \times 10^{-3}$ and $J_{\rm GW}/M^2 = 3.545(3.546) \times 10^{-2}$; for $r_p = 15$ and 20 $(E_{\rm GW}/M, J_{\rm GW}/M^2) = (1.64 \times 10^{-4}, 8.69 \times 10^{-3})$ and $(3.8 \times 10^{-5}, 2.8 \times 10^{-3})$, respectively. Taking this as orbital energy and angular momentum loss gives a Newtonian estimate for the time to the next close encounter of 65 ms for the $r_p = 10$ case. For the next largest impact parameter simulated, $r_p = 15$, the tidal deformation is negligible, and the estimated time to the next close encounter is 1.8 s. This suggests precursor EM transients associated with crust shattering for these systems could be produced of order hundreds of milliseconds, but probably not more than a few seconds, before merger.

For the intermediate cases ($r_p = 7.5$ and 8.75), the stars come into contact and form a single object. For $r_p = 7.5$, this happens at the first close encounter; for $r_p = 8.75$, the stars briefly fly apart before merging. When the stars come into contact they undergo shock heating and develop features similar to the Kelvin–Helmholtz vortices observed in Rosswog et al. (2012; see Figure 3). Though the total mass is above the maximum for a cold, static star with this EOS, the stars are highly spun-up and have a significant thermal component (22%–25%) to their internal energy (see Table 1). In the vicinity of these objects the (density-weighted) average thermal specific energy is $\epsilon_{\rm th} \approx$ 10–20 MeV/m_n where m_n is the neutron mass.

These HMNSs produce quasi-periodic GWs with frequency ~ 3.2 kHz (see Figure 2). Though these hypermassive configurations survive the duration of our simulations (≈ 13 ms), they presumably will eventually collapse to form BHs. In Table 1, we indicate the rate of energy and angular momentum loss to GWs at the end of the simulation. From this one can roughly estimate the time it will take for the HMNS to radiate its remaining angular momentum to GWs assuming a constant $dJ_{\rm GW}/dt$ (e.g., for the $r_p = 7.5$, HB case, it will take ~ 70 ms). However, magnetohydrodynamic effects, such as the magnetorotational instability, as well as cooling by neutrino emission, none of which we take into account, will also be important in determining when these stars collapse. Table 1 also lists data from the unequal mass ratio ($q = 0.8$), $r_p = 7.5$ case, which shows qualitatively similar behavior to the equal mass case.

3.2. *Effect of Equation of State*

In addition to the HB EOS, we also simulated an intermediate impact parameter $r_p = 7.5$ using the B (softer) and 2H (stiffer) EOSs. For the B EOS, a BH forms soon after merger with $M_{\rm BH}/M = 0.988$ and $a = 0.766$; the total radiated energy and angular momentum are $E_{\rm GW}/M = 3.55 \times 10^{-2}$ and $J_{\rm GW}/M^2 = 0.239$, respectively. For the 2H EOS, the total mass is below the maximum for a stable cold NS and the stars fly apart after the first collision before eventually settling down to a single massive star.

We also performed simulations with the B and 2H EOSs and $r_p = 10$. With the softer B EOS, the NSs undergo a close encounter that is qualitatively similar to the HB EOS. However, because of the greater compactness of the NS, the amplitude of the resulting GW pulse is larger with 19% and 13% more energy and angular

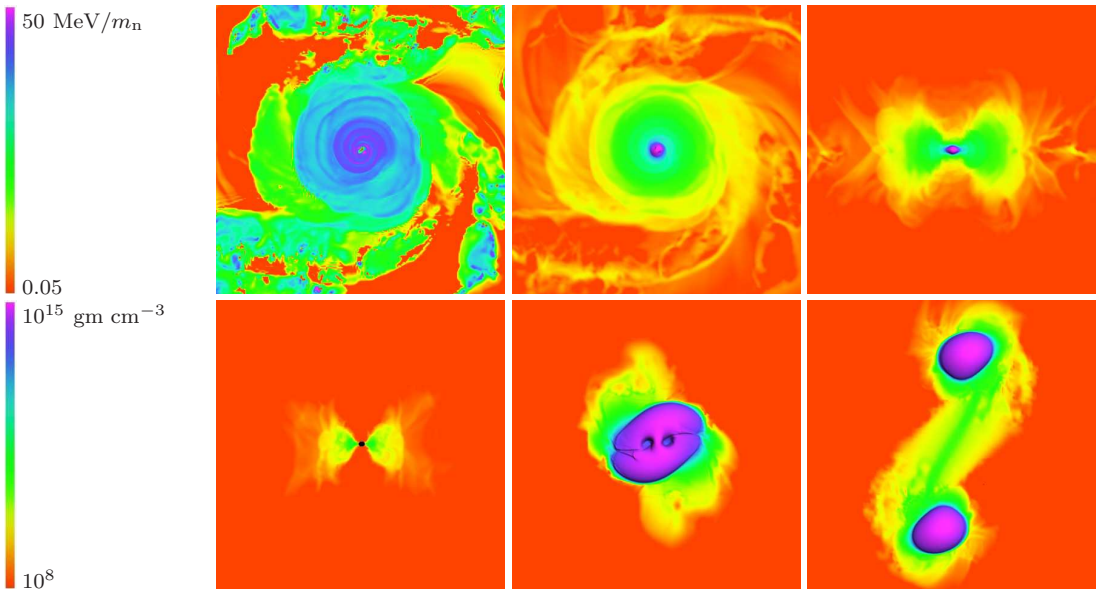

FIG. 3.— Snapshots of thermal specific energy (top left panel) with a logarithmic color scale from 0.05 to 50 MeV/$m_{\rm n}$ and rest-mass density (other five panels) from 10^8 to 10^{15} gm cm^{-3}. The top left and top middle, and bottom middle and bottom right panels show the equatorial plane, while the other two show a perpendicular plane through the center of mass. The top panels show an HMNS with surrounding disk and unbound material from the $r_p = 8.75$, HB EOS case at $t = 13.3$ ms. The bottom panels show, from left to right, a BH and a surrounding disk for the $r_p = 7.5$ B EOS case at $t = 10.2$ ms; a merger from the $r_p = 7.5$, HB EOS case at $t = 3.2$ ms; NSs with excited f-mode perturbations post close encounter from the $r_p = 10$, HB EOS case at $t = 4.1$ ms. The first four panels have the same distance scale, where the coordinate radius of the HMNS and BH are ≈ 13 and ≈ 6 km, respectively. The last two panels share a second distance scale; the coordinate separation between the NSs in the last panel is ≈ 73 km.

r_p	EOS	$J_{\rm tot}/M^2$ [a]	$\langle\epsilon_{\rm th}\rangle$ [b]	$E_{\rm th}/E_{\rm int}$ [c]	$M_{0,u}$ [d]	$\frac{E_{\rm GW}}{M}\times 100$ [e]	$\frac{J_{\rm GW}}{M^2}\times 100$ [f]	$dE_{\rm GW}/dt$ [g]	$dJ_{\rm GW}/dt/M$ [h]
7.5	HB	0.96	20	0.22	0.64	3.78(3.91)	30.5(31.2)	1.56×10^{-5}	1.23×10^{-4}
7.5 ($q=0.8$)	HB	0.96	14	0.17	0.57	3.36	27.5	7.60×10^{-6}	6.22×10^{-5}
7.5	2H	0.95	14	0.31	4.39	0.70	10.8	3.45×10^{-7}	3.20×10^{-6}
8.75	HB	1.05	17	0.25	2.65	2.07	24.0	1.50×10^{-5}	1.14×10^{-4}
10	2H	1.11	11	0.27	6.65	0.50	9.28	2.70×10^{-6}	3.48×10^{-5}

TABLE 1
PROPERTIES OF HYPERMASSIVE NS CASES, MEASURED AT $t \approx 13.3$MS

[a] Global angular momentum.
[b] Density-weighted average of the thermal component of the specific energy in units of MeV/m_n.
[c] Fraction of internal (Eulerian) energy that is thermal.
[d] Rest mass that is unbound in percent of $M_\odot$.
[e] The total energy emitted in GWs through the $r = 100M$ surface.
[f] The total angular momentum emitted in GWs.
[g] Average GW flux of energy.
[h] Average GW flux of angular momentum.

momentum, respectively. Due to the large eccentricity, this will have a significant effect on the subsequent orbit of the NSs. The estimate of the time to the next close encounter is 50 ms with the B compared to 65 ms for the HB EOS. Binaries with impact parameters in this range may undergo multiple close encounters before merging, with the time between the GW bursts a sensitive function of (in this example) the EOS. For the 2H EOS, the stars have larger radii and graze during the close encounter, merging to a massive star soon after.

3.3. *Possible Post-merger Transients*

Intermediate impact parameters ($r_p = 7.5$ for the various EOSs and mass ratios, $r_p = 8.75$ HB, and $r_p = 10$ 2H EOS) form HMNSs with non-negligible accretion disks, thought to be necessary for an SGRB progenitor, and unbound material which could potentially power other EM transients (as would presumably a subset of larger impact parameter systems were we to follow them through merger). Figure 4 shows the amount of matter, total and unbound (fluid cells with outward radial velocity and four-velocity time component $u_t < -1$; see also Table 1), outside a given radius from the center of mass and the velocity distribution of the unbound matter. The various cases have 0.005–0.07$M_\odot$ unbound material, and roughly 2–3 times more in a disk. As expected, cases with less compact NSs have more unbound material compared to more compact cases. Larger impact parameters (which have more angular momentum) also have comparatively more unbound material with the most occurring in cases where the NSs first come into contact in non-merger close encounters ($r_p = 8.75$ HB and $r_p = 7.5$ and 10 2H). The unequal mass-ratio merger with $q = 0.8$ produces slightly less unbound material than the com-

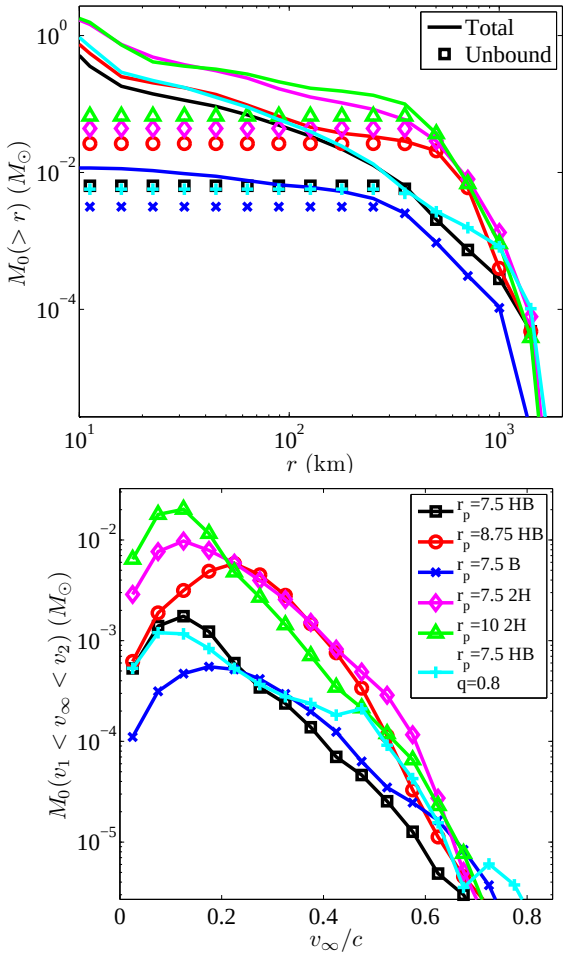

FIG. 4.— Top: the total and unbound rest mass outside a given radius from the center of mass for various cases at $t \approx 13$ ms. Bottom: unbound rest mass with asymptotic velocity grouped in $0.05c$ bins. The legend applies to the top panel as well. By this time, the $r_p = 7.5$, B case has collapsed to a BH, the $r_p = 7.5$, 2H case is an NS below the maximum mass for this EOS, while the rest are HMNSs.

parable equal mass merger. In all cases, the ejecta is mildly relativistic with asymptotic velocity that peaks in the range 0.1–0.3c. This ejecta is presumably neutron rich and will convert to heavy elements through the r-process, the heaviest of which will undergo fission, emitting photons (Li & Paczynski 1998; Kulkarni 2005; Metzger et al. 2010). The arguments from Metzger et al. (2010) estimate the time scale as

$$t_{\rm peak} \approx 0.6\ {\rm d}(M_{\rm u}/3\times10^{-2}M_\odot)^{1/2}(v/0.2c)^{-1/2}$$

with a luminosity, peaking in the optical/near UV, of

$$L \approx 4\times10^{42}\ {\rm erg\ s^{-1}}(M_{\rm u}/3\times10^{-2}M_\odot)^{1/2}(v/0.2c)^{1/2}$$

normalized here to the approximate values from the $r_p = 8.75$ case. However, recent calculations using more detailed heavy element opacities suggest that the timescale may be up to a week with emission peaking in the IR (Kasen 2012).

This ejecta is also expected to collide with the interstellar medium producing radio waves that will peak on timescales of weeks with brightness (Nakar & Piran 2011)

$$F(\nu_{\rm obs}) \approx 0.4(E_{\rm kin}/2\times10^{51}\ {\rm erg})(n_0/0.1{\rm cm^{-3}})^{7/8}$$
$$(v/0.2c)^{11/4}(\nu_{\rm obs}/{\rm GHz})^{-3/4}(d/100{\rm Mpc})^{-2}\ {\rm mJy}$$

where n_0 is the density of the surrounding environment (we use $n_0 \sim 0.1$ cm^{-3} for GC cores; Rosswog et al. 2012), $\nu_{\rm obs}$ is the observation frequency, d the distance, and we have normalized the kinetic energy and velocity to the $r_p = 8.75$, HB simulation.

4. CONCLUSIONS

We have performed GRHD simulations modeling dynamical capture NS–NS mergers, giving direct estimates of the corresponding GW emission and merger outcome varying impact parameter, EOS, and mass ratio. By measuring pre-merger tidal deformation and post-merger stripped material (bound and ejected), we have also speculated on related EM transients.

Regarding transients that may precede the merger, non-merging close encounters can lead to tidal deformations strong enough to crack the NSs' crust and tap into the $\sim 10^{46}$ erg stored in elastic energy (Thompson & Duncan 1995), potentially causing flaring activity from milliseconds up to possibly a few seconds before merger. Though a different mechanism and time scales, the signature could be similar to resonance induced cracking for quasi-circular inspirals proposed in Tsang et al. (2012). The cracking of the NS crust is one possible explanation for SGRB precursors observed by *Swift* (Troja et al. 2010).

We find that dynamical capture mergers can result in prompt BH formation or the formation of an HMNS depending on impact parameter and EOS. The HMNSs will be long lived due to their rapid rotation and thermal energy, giving them the potential to seed large magnetic fields and source intense transients during collapse.

In contrast to what was found in general-relativistic studies of quasi-circular NS–NS mergers, we find that dynamical capture mergers can result in massive disks even for equal mass binaries, and can result in up to a few percent of a solar mass in ejecta. This mildly relativistic ejecta can produce potentially observable optical and radio transients. The amount of ejecta found here is similar to the 0.009–0.06 $M_\odot$ found with Newtonian gravity (Rosswog et al. 2012), though not for comparable impact parameters ($r_p \leq 5$). However, what is qualitatively consistent with the Newtonian setups is that we observe the largest amounts of unbound material for grazing collisions.

Regarding GW detectability, the high frequency of the merger-ringdown or quasi-periodic signals from the HMNS will be difficult to observe with AdLIGO. Individual bursts from close encounters would also not be detectable except for very nearby events. For example, an $r_p = 10$, HB EOS merger at $d = 100$ Mpc has sky-averaged S/N for AdLIGO of ≈ 0.9. This implies that if dynamical capture NS–NS mergers constitute a fraction of SGRB progenitors, a further subset of these will not have a detectable GW counterpart. GW signals from larger r_p binaries undergoing numerous close encounters would have larger S/N, and the timing between bursts will be a sensitive function of the orbital energy, containing information about the EOS, for ex-

ample. We defer a detailed study of GW detectability to future work (East et al. 2012a).

We thank Chris Thompson for useful discussions, as well as participants of the KITP "Rattle and Shine" conference (2012 July). This research was supported by NSF grant PHY-0745779, and resources from NSF XSEDE provided by NICS under grant TG-PHY100053 and the Orbital cluster at Princeton University.

REFERENCES

Abramovici et al., A. 1992, Science, 256, 325
Antonini, F., & Perets, H. B. 2012, ApJ, 757, 27
Arcones, A., & Janka, H.-T. 2011, A&A, 526, A160
Dull, J. D., Cohn, H. N., Lugger, P. M., Murphy, B. W., Seitzer, P. O., Callanan, P. J., Rutten, R. G. M., & Charles, P. A. 1997, ApJ, 481, 267
——. 2003, ApJ, 585, 598, arXiv:astro-ph/0210588
East, W. E., McWilliams, S. T., Levin, J., & Pretorius, F. 2012a, in prep.
East, W. E., Pretorius, F., & Stephens, B. C. 2012b, Phys. Rev. D, 85, 124009
——. 2012c, Phys. Rev. D, 85, 124010
East, W. E., Ramazanoğlu, F. M., & Pretorius, F. 2012, ArXiv e-prints, 1208.3473
Faber, J. A., & Rasio, F. A. 2012, ArXiv e-prints, 1204.3858
Fabian, A. C., Pringle, J. E., & Rees, M. J. 1975, MNRAS, 172, 15P
Fischer, T., Whitehouse, S. C., Mezzacappa, A., Thielemann, F.-K., & Liebendörfer, M. 2010, A&A, 517, A80
Gold, R., Bernuzzi, S., Thierfelder, M., Bruegmann, B., & Pretorius, F. 2011, ArXiv e-prints, 1109.5128
Grindlay, J., Portegies Zwart, S., & McMillan, S. 2006, Nature Physics, 2, 116, arXiv:astro-ph/0512654
Horowitz, C. J., & Kadau, K. 2009, Phys. Rev. Lett., 102, 191102
Kaiser, N. 2004, in SPIE Conference Series, Vol. 5489, ed. J. M. Oschmann Jr., 11–22
Kasen, D. 2012, in work presented at KITP 'Rattle and Shine' conference
Kocsis, B., & Levin, J. 2012, Phys. Rev. D, 85, 123005, 1109.4170
Kulkarni, S. R. 2005, ArXiv Astrophysics e-prints, arXiv:astro-ph/0510256
Lattimer, J. M., & Schramm, D. N. 1974, ApJ, 192, L145
Lee, W. H., Ramirez-Ruiz, E., & van de Ven, G. 2010, ApJ, 720, 953, 0909.2884
Lehner, L., Palenzuela, C., Liebling, S. L., Thompson, C., & Hanna, C. 2011, ArXiv e-prints, 1112.2622
Li, L.-X., & Paczynski, B. 1998, Astrophys.J., 507, L59, astro-ph/9807272
LSST Science Collaborations et al. 2009, ArXiv e-prints, 0912.0201
Metzger, B. D., & Berger, E. 2012, ApJ, 746, 48, 1108.6056
Metzger, B. D. et al. 2010, MNRAS, 406, 2650, 1001.5029
Murphy, B. W., Cohn, H. N., & Lugger, P. M. 2011, ApJ, 732, 67, 1205.1049
Nakar, E., & Piran, T. 2011, Nature, 478, 82, 1102.1020
O'Leary, R. M., Kocsis, B., & Loeb, A. 2009, MNRAS, 395, 2127, 0807.2638
Peters, P., & Mathews, J. 1963, Phys. Rev., 131, 435
Pfahl, E., Rappaport, S., & Podsiadlowski, P. 2002, ApJ, 573, 283, arXiv:astro-ph/0106141
Piran, T., Nakar, E., & Rosswog, S. 2012, ArXiv e-prints, 1204.6242
Press, W. H., & Teukolsky, S. A. 1977, ApJ, 213, 183
Rau, A. e. a. 2009, PASP, 121, 1334, 0906.5355
Read, J. S., Markakis, C., Shibata, M., Uryū, K., Creighton, J. D. E., & Friedman, J. L. 2009, Phys. Rev. D, 79, 124033, 0901.3258
Roberts, L. F., Kasen, D., Lee, W. H., & Ramirez-Ruiz, E. 2011, The Astrophysical Journal Letters, 736, L21
Rosswog, S., Piran, T., & Nakar, E. 2012, ArXiv e-prints, 1204.6240
Rosswog, S., Thielemann, F. K., Davies, M. B., Benz, W., & Piran, T. 1998, in Nuclear Astrophysics, ed. W. Hillebrandt & E. Muller, 103, arXiv:astro-ph/9804332
Sekiguchi, Y., Kiuchi, K., Kyutoku, K., & Shibata, M. 2011, Phys. Rev. Lett., 107, 051102
Stephens, B. C., East, W. E., & Pretorius, F. 2011, ApJ, 737, L5, 1105.3175
Thompson, C., & Duncan, R. C. 1995, MNRAS, 275, 255
Thompson, T. A. 2011, Astrophys.J., 741, 82, 1011.4322
Troja, E., Rosswog, S., & Gehrels, N. 2010, The Astrophysical Journal, 723, 1711
Tsang, D., Read, J. S., Hinderer, T., Piro, A. L., & Bondarescu, R. 2012, Phys. Rev. Lett., 108, 011102